Imaging Near-surface Heterogeneities by Natural Migration of Surface Waves

Zhaolun Liu, Abdullah AlTheyab, Sherif M. Hanafy, and Gerard Schuster, King Abdullah University of Science and Technology (KAUST)*

SUMMARY

We demonstrate that near-surface heterogeneities can be imaged by natural migration of backscattered surface waves in common shot gathers. No velocity model is required because the data are migrated onto surface points with the virtual Green's functions computed from the shot gathers. Migrating shot gathers recorded by 2D and 3D land surveys validates the effectiveness of detecting near-surface heterogeneities by natural migration. The implication is that more accurate hazard maps can be created by migrating surface waves in land surveys.

INTRODUCTION

The scattered surface wave generated by strong heterogeneities in the shallow subsurface is often seen as noise in seismic reflection exploration (Blonk et al., 1995; Ernst et al., 2002). However, this noise can also be used as signal if the backscattered data is migrated to image the near-surface heterogeneities (Snieder, 1986; Riyanti, 2005; Yu et al., 2014; Hyslop and Stewart, 2015).

The relations between the model perturbation $\mathbf{m}$ and the backscattered surface waves $\mathbf{d}$ can be linearized by the Born approximation $\mathbf{d} = \mathbf{L}\mathbf{m}$, where $\mathbf{L}$ is the forward modeling operator for a known background velocity (Snieder, 1986; Tanimoto, 1990). To get the model perturbation $\mathbf{m}$, Riyanti (2005) used an iterative optimization method to approximate the solution, and Snieder (1986) and Yu et al. (2014) applied the adjoint of the forward modeling operator $\mathbf{L}^\dagger$ to backscattered data to obtain the migration image.

Recently, AlTheyab et al. (2015, 2016) introduced the natural migration (NM) method to image the near-surface heterogeneities, assuming that the scattering bodies are within a depth of about 1/2 wavelength. This also assumes that sources and receivers are densely distributed to avoid aliasing artifacts in the migration image.

There are several benefits of the NM method. First, no Born approximation is used so that strongly scattered events can be migrated to their place of origin, namely the fault locations are projected onto the surface. Second, no velocity model is needed because the Green's functions in the migration kernel are recorded as band-limited shot gathers, where the sources and receivers are located on the surface. Third, this method is called a natural migration equation because the Green's functions are estimated from the shot gathers recorded by a dense array of seismometers. If the trial image point is on or near the surface then no velocity model is required and so there will be no mispositioning errors in the migration images.

AlTheyab et al. (2016) demonstrated the effectiveness of surface-wave migration with ambient noise data, but did not show it to be effective for controlled source data. This paper now shows the results of applying natural surface wave migration to controlled source data recorded over areas with near-surface faults. Results show that migration of back-scattered surface waves can detect the presence of near-surface heterogeneities, which can indicate the existence of faults or low velocity zones (LVZ).

THEORY OF NATURAL MIGRATION

Assume Rayleigh-wave scattering recorded along the vertical component and excited by a bandlimited vertical point source. In this case, the natural migration equation in the frequency domain can be expressed as (AlTheyab et al., 2016),

$$m(\mathbf{x}') = \sum_{s,r\in B} \int 2\omega^2 W(\omega)^* G(\mathbf{x}'|\mathbf{x}_s)^* G(\mathbf{x}'|\mathbf{x}_r)^* u(\mathbf{x}_s,\mathbf{x}_r) d\omega, \tag{1}$$

where $m(\mathbf{x}')$ is the perturbation model that represents an arbitrary distribution of elastic-parameter perturbations at the image point $\mathbf{x}'$; ω is the angular frequency; $W(\omega)$ is the source-wavelet spectrum; $*$ is the complex-conjugate symbol; $\mathbf{x}'$, $\mathbf{x}_s$ and $\mathbf{x}_r$ are, respectively, the migration image, source and receiver positions at the free surface locations in the set B; $G(\mathbf{x}'|\mathbf{x}_s)$ is the monochromatic Green's function for the vertical-component source at $\mathbf{x}_s$ and receiver at $\mathbf{x}'$, and $G(\mathbf{x}'|\mathbf{x}_r)$ is the transmitted-wave Green's function for a vertical-component particle velocity recording that only contains the transmitted wavefield without backscattering; $u(\mathbf{x}_s,\mathbf{x}_r)$ is the particle displacement.

The active-source wavelet spectrum is $W(\omega)$, so the wavefield $u(\mathbf{x}'|\mathbf{x}_s)$ can be expressed as $W(\omega)G(\mathbf{x}'|\mathbf{x}_s)$ and the Green's function can be expressed as,

$$G(\mathbf{x}'|\mathbf{x}_s) = u(\mathbf{x}'|\mathbf{x}_s)W(\omega)^{-1}. \tag{2}$$

Substituting equation 2 into the migration equation 1 gives the natural migration equation for active data,

$$\begin{aligned} m(\mathbf{x}') &= \sum_{s,r} \int 2\omega^2 \left[W(\omega)^{-1} u(\mathbf{x}'|\mathbf{x}_s) u(\mathbf{x}'|\mathbf{x}_r)\right]^* u(\mathbf{x}_s,\mathbf{x}_r) d\omega \\ &= \sum_{s,r} \int L(\mathbf{x}_r|\mathbf{x}'|\mathbf{x}_s)^* u(\mathbf{x}_s,\mathbf{x}_r) d\omega, \end{aligned} \tag{3}$$

where $L(\mathbf{x}_r|\mathbf{x}'|\mathbf{x}_s) = 2\omega^2 W(\omega)^{-1} u(\mathbf{x}'|\mathbf{x}_s) u(\mathbf{x}'|\mathbf{x}_r)$ is the forward modeling kernel. To calculate $L(\mathbf{x}_r|\mathbf{x}'|\mathbf{x}_s)$, the source wavelet $W(\omega)$ must be estimated and then it is used to form the deconvolution filter $W(\omega)^{-1}$.

The migration image $m(\mathbf{x}')$ for $\mathbf{x}' \in B$ in equation 3 can be seen as the projection of the scatterer at shallow depths onto the free surface denoted by the set of points B (Campman et al., 2005). Therefore, migration images can be mapped to different depths

in the medium because surface waves at lower frequencies are more sensitive to deeper scatterers. So, u in equation 3 should be filtered by a narrow-band filter prior to migration.

According to AlTheyab et al. (2016), the transmitted and backscattered surface waves can be separated by muting and all arrivals within one wavelength of the source position should be muted. Figure 1 shows the corresponding NM workflow for active data.

NUMERICAL RESULTS

Results are now shown for natural migration of surface waves for both synthetic data and field data. The field data are recorded for land surveys near Aqaba, Jordan and the Qademah fault system in Saudi Arabia. The workflow for migrating the surface waves with equation 3 is shown in Figure 1. Additional details are given in AlTheyab et al. (2016).

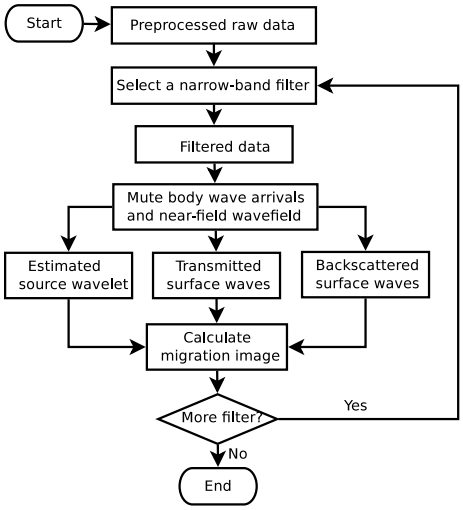

Figure 1: The natural migration workflow for active-source data.

Natural Migration of Synthetic Data

Synthetic shot gathers were computed by finite-difference solutions to the 2D elastic wave equation. The peak frequency of the source wavelet is 10 Hz, and each shot gather consisted of 200 traces, with the trace spacing of 3 meter. The input earth model is the simple fault model shown in Figure 2, and the input data consist of 200 z-component shot gathers with a 3-meter shot spacing. The shots are particle-velocity displacements along the z-component at points along the surface.

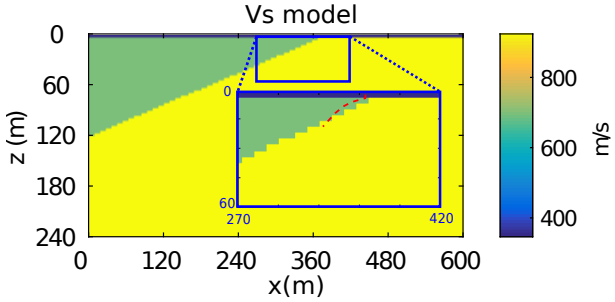

Figure 2: Simple fault velocity model used for the synthetic tests, where the area in the blue rectangle is enlarged.

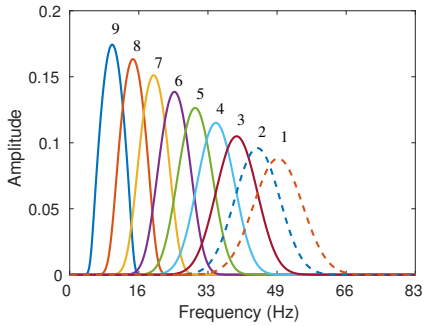

Figure 3: The amplitude spectra of nine filters used for the synthetic data before natural migration.

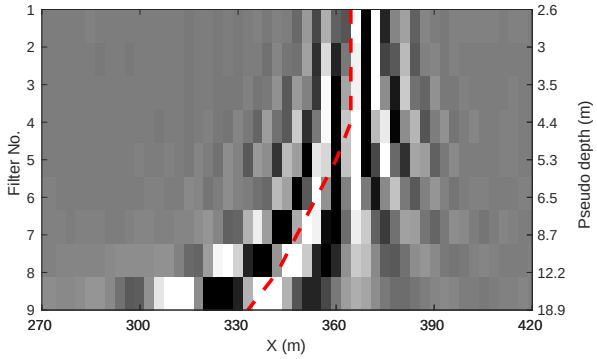

Figure 4: The normalized stacked migration images at $z = 0$ and x from 270 m to 420 m, and computed from the synthetic data with different narrow-band filters. The right y axis is pseudo depth calculated from 1/3 the wavelength, and the red dashed line is the interpreted fault position corresponding to the red dash line in Figure 2.

Nine narrow-band filters (the center frequency changes from 10 Hz to 50 Hz with a 5 Hz interval) are designed to identify the depth anomalies in the model, and their amplitude spectra are shown in Figure 3. The z-component traces were migrated according to equation 3 and the stacked migration images are shown in Figure 4. We can see that the migration results show that the location of the fault changes with frequency. The migration image for higher frequency data delineates the shallow part of the fault, while the deep part of the fault is imaged from the lower-frequency data. The depth of each migration image can be estimated by assigning each center frequency to the depth of about 1/3 the wavelength. By mapping the red dashed line onto the Vs model shown in Figure 2, we can see that the migration image delineates the approximate dip of the fault.

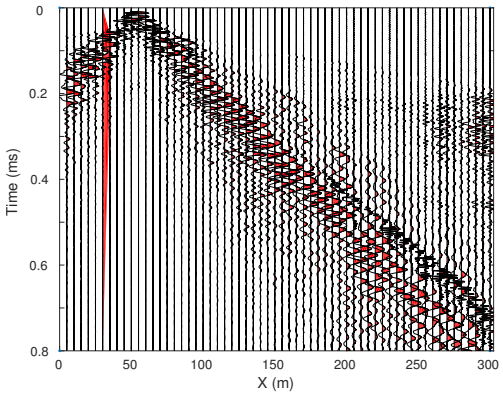

Figure 5: Common shot gather from the Aqaba data.

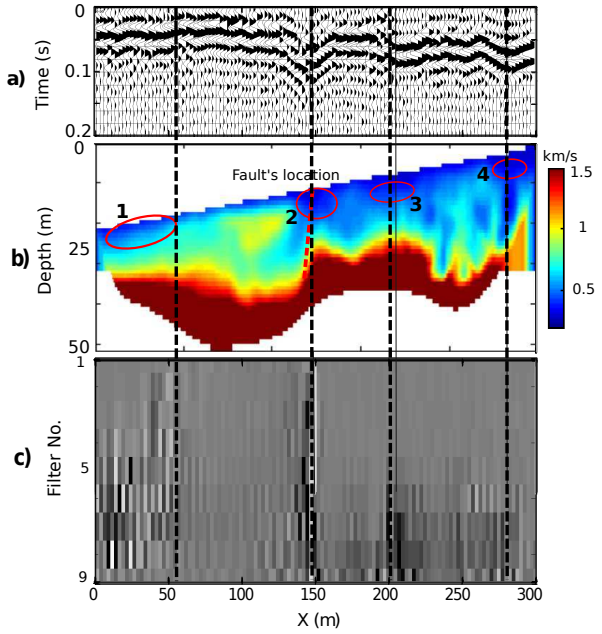

Figure 6: a) Common offset gather (COG) with 7.5 m offset, b) traveltime tomogram, and c) stacked surface-wave migration images for the Aqaba data with nine narrow-band filters. The locations denoted by 2-4 are clearly associated with horizontal velocity anomalies in all three illustrations; the horizontal velocity anomaly denoted by location 1 also seen in the traveltime tomogram.

Natural Migration of Aqaba Data

A 2D land survey was carried out along the Red Sea coast near Aqaba, Jordan. There were 120 shot gathers recorded, with shot and receiver intervals of 2.5 m. The source is a 40-kg weight drop striking a metal plate on the ground. A typical shot gather is shown in Figure 5.

Migrating the surface waves to the free surface after applying nine narrow-band filters to the shot gathers (the center frequency changes from 15 Hz to 55 Hz with 5 Hz interval, where parts of the amplitude spectra are shown in Figure 3.) gives the migration images in Figure 6c. In all the migration images, the main fault is located at $x = 150$ m on the surface, which is also observed in the field as the surface expression of a strike-slip fault.

There are two other velocity anomalies at $x = 205$ m and $x = 280$ m (locations 3 and 4 in Figure 6b) in Figure 6c that are detected in the lower-frequency migration images, which means that they are deeper velocity anomalies. The traveltime tomogram shown in Figure 6b suggests that there are faults or low-velocity zones (LVZs) at these locations. The low-velocity zones are clearly seen in the common offset gathers at $x = 200$ m and $x = 280$ m in Figure 6a, where abrupt changes in velocity are accompanied by sharp changes in the arrival times of the surface waves. There also exists velocity anomalies located at $x =$ from 0 to 50 m, which can be seen in the traveltime tomogram.

This example illustrates that the surface-wave migration image can be interpreted at the locations of abrupt velocity changes in the tomogram, which can represent the existence of either a LVZ or a near-surface fault. For the anomaly at x=150 m, this anomaly is that of a strike-slip fault.

Natural Migration of Qademah Data

A 3D land survey was carried out along the Red Sea coast over the Qademah fault system, about 30 km north of the KAUST campus. There were 288 receivers arranged in 12 parallel lines, and each line has 24 receivers. The inline receiver interval is 5 m and the crossline interval is 10 m. The receiver geometry is shown in Figure 7a, where one shot is fired at each receiver location for a total of 288 shot gathers. The source is a 200-lb hammer striking a metal plate on the ground, and a shot gather is shown in Figure 7b.

Applying equation 3 to 288 shot gathers gives the stacked migration image in Figure 8 with eight narrow-band filters shown in Figure 9. The black arrows in Figure 8 show the images of near-surface heterogeneities by using the filters from 4 to 7, and the positions of these images change from about 45 m to 85 m with increasing frequency (can be seen as depth) in the data, which agrees very well with the actual fault location indicated by traveltime tomography (Hanafy et al., 2015). The low-frequency filter 7 suggests that the fault is at least as deep as $\lambda/3 = 7$ m.

CONCLUSIONS

Synthetic data and field records are used to demonstrate that near-surface heterogeneities can be imaged by natural migration of backscattered surface waves in common shot gathers. No velocity model is required because the data are migrated with the virtual Green's functions computed from the shot gathers. Migrating shot gathers recorded by 2D and 3D land surveys validates the effectiveness of detecting faults by natural migration. The implication is that more accurate hazard maps can be created by migrating surface waves in land surveys.

A limitation of surface-wave migration is that the migration image on the surface has an ambiguous interpretation, and it

can represent either a LVZ or a near-surface fault. To reduce this uncertainty, we suggest the use of least squares migration with image points at depth. However, this requires knowledge of the S-velocity distribution in depth and inverting the surface waves for the S-velocity model.

ACKNOWLEDGMENTS

The research reported in this publication was supported by the King Abdullah University of Science and Technology (KAUST) in Thuwal, Saudi Arabia. We thank the sponsors of the CSIM consortium for their support. We would also like to thank the high performance computing (HPC) center of KAUST for providing access to super computing facilities.

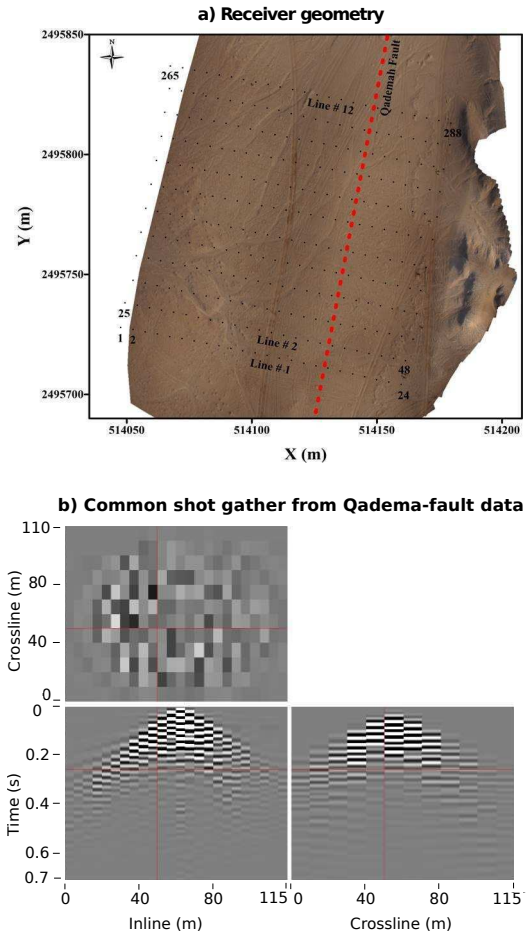

Figure 7: a) Receiver geometry and b) common shot gather from the Qadema-fault data. Shots were located at each geophone, and a total of 288 shot gathers were migrated using equation 3. The Qadema fault is located along the dashed red line (Hanafy et al., 2015).

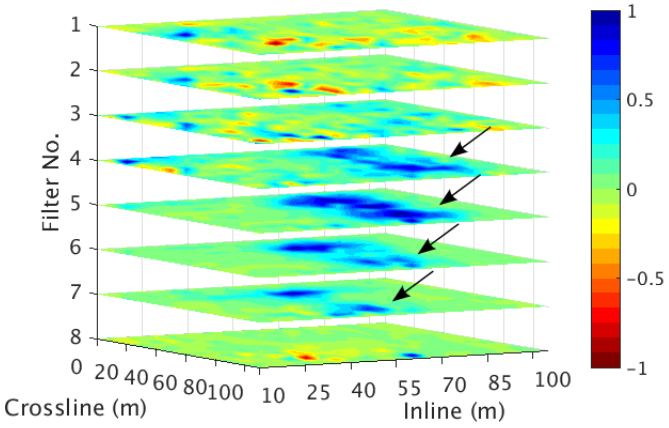

Figure 8: Stacked migration images for the Qadema-fault data filtered by eight narrow-band filters. The location of the Qademah fault indicated by the black arrows are correlated with the S-velocity tomogram shown in Figure 10. There is no visible indication of the fault on the free surface.

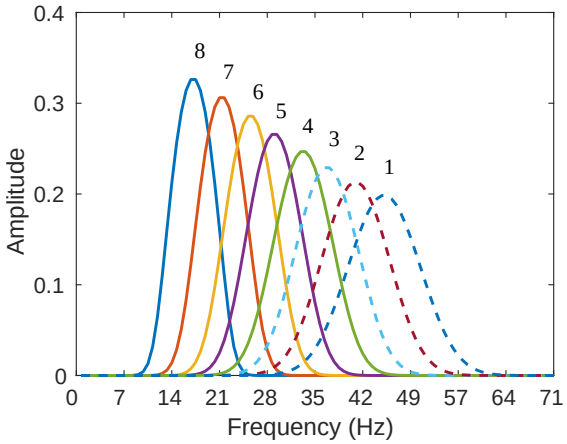

Figure 9: The spectra of eight narrow-band filters used for the natural migration of Qademah data.

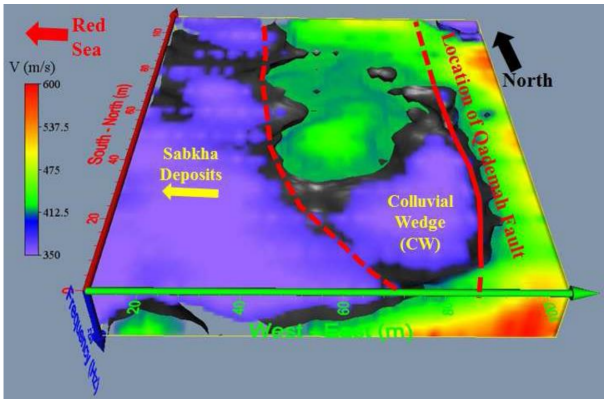

Figure 10: The 3D Rayleigh phase velocity tomogram (Hanafy et al., 2015).

EDITED REFERENCES

Note: This reference list is a copyedited version of the reference list submitted by the author. Reference lists for the 2016 SEG Technical Program Expanded Abstracts have been copyedited so that references provided with the online metadata for each paper will achieve a high degree of linking to cited sources that appear on the Web.

REFERENCES

AlTheyab, A., F. Lin, and G. Schuster, 2016, Imaging near-surface heterogeneities by natural migration of back-scattered surface waves: Geophysical Journal International, **204**, 1332–1341, http://dx.doi.org/10.1093/gji/ggv511.

AlTheyab, A., E. Workman, F. Lin, and G. Schuster, 2015, Imaging near-surface heterogeneities by natural migration of back-scattered surface waves: 77th Annual International Conference and Exhibition, EAGE, Extended Abstracts, http://dx.doi.org/10.3997/2214-4609.201413572.

Blonk, B., G. C. Herman, and G. G. Drijkoningen, 1995, An elastodynamic inverse scattering method for removing scattered surface waves from field data: Geophysics, **60**, 1897–1905, http://dx.doi.org/10.1190/1.1443921.

Campman, X. H., K. van Wijk, J. A. Scales, and G. C. Herman, 2005, Imaging and suppressing near-receiver scattered surface waves: Geophysics, **70**, no. 2, V21–V29, http://dx.doi.org/10.1190/1.1884831.

Ernst, F. E., G. C. Herman, and A. Ditzel, 2002, Removal of scattered guided waves from seismic data: Geophysics, **67**, 1240–1248, http://dx.doi.org/10.1190/1.1500386.

Hanafy, S. M., 2015, Mapping the Qademah fault with traveltime, surface-wave, and resistivity tomograms: 85th Annual International Meeting, SEG, Expanded Abstracts, 3347–3351.

Hyslop, C., and R. R. Stewart, 2015, Imaging lateral heterogeneity using reflected surface waves: Geophysics, **80**, no. 3, EN69–EN82, http://dx.doi.org/10.1190/geo2014-0066.1.

Riyanti, C. D., 2005, Modeling and inversion of scattered surface waves: Ph.D. thesis, Delft University of Technology, TU Delft.

Snieder, R., 1986, 3-D linearized scattering of surface waves and a formalism for surface wave holography: Geophysical Journal International, **84**, 581–605, http://dx.doi.org/10.1111/j.1365-246X.1986.tb04372.x.

Tanimoto, T., 1990, Modelling curved surface wave paths: Membrane surface wave synthetics: Geophysical Journal International, **102**, 89–100, http://dx.doi.org/10.1111/j.1365-246X.1990.tb00532.x.

Yu, H., B. Guo, S. Hanafy, F.-C. Lin, and G. T. Schuster, 2014, Direct detection of near-surface faults by migration of back-scattered surface waves: 84th Annual International Meeting, SEG, Expanded Abstracts, 2135–2139, http://dx.doi.org/10.1190/segam2014-0737.1.